MATHEMATICAL BIOSCIENCES
AND ENGINEERING
Volume **9**, Number **1**, January **2012**

doi:10.3934/mbe.2012.9.61

pp. **61–74**

AN EVALUATION OF DYNAMIC OUTLET BOUNDARY CONDITIONS IN A 1D FLUID DYNAMICS MODEL

Rachel Clipp

1) Department of Biomedical Engineering
North Carolina State University, Raleigh, NC 27695-7115, USA
2) Applied Research Associates, Inc
8537 Six Forks Road, Suite 600
Raleigh, NC 27615, USA

Brooke Steele

Department of Biomedical Engineering
Engineering Building 3, RM 4204B
North Carolina State University, Raleigh, NC 27695-7115, USA

(Communicated by Mette Olufsen)

Abstract. When modeling the cardiovascular system, the use of boundary conditions that closely represent the interaction between the region of interest and the surrounding vessels and organs will result in more accurate predictions. An often overlooked feature of outlet boundary conditions is the dynamics associated with regulation of the distribution of pressure and flow. This study implements a dynamic impedance outlet boundary condition in a one-dimensional fluid dynamics model using the pulmonary vasculature and respiration (feedback mechanism) as an example of a dynamic system. The dynamic boundary condition was successfully implemented and the pressure and flow were predicted for an entire respiration cycle. The cardiac cycles at maximal expiration and inspiration were predicted with a root mean square error of 0.61 and 0.59 mm Hg, respectively.

1. **Introduction.** Mathematical models can be used to improve our understanding of physical systems. Sufficiently accurate computer models of the cardiovascular system may be used to design improved treatment options by predicting blood flow distribution and pressure due to disease [23, 24] or as a result of surgical intervention [24, 27, 32]. While the potential of computational modeling to improve patient care is tremendous, several challenges must be overcome before predictive models can be included in routine clinical use. In this work, we describe how to incorporate downstream (i.e., distal) dynamic phenomena into a local hemodynamic model of blood flow and pressure. This method may be used to consider the effects caused by regulatory or feedback mechanisms in specific organ systems, such as respiration [3, 20, 34] or pressure regulation within the renal system [7, 19]. These regulatory mechanisms can modulate flow, maintain pressure (i.e., renal nephrons) or cause pressure increases due to the interaction between two physiologic systems (i.e. pulmonary arterioles and alveoli). The inclusion of distal dynamics may improve the

2000 *Mathematics Subject Classification.* Primary: 82C21, 92C35, 74S05; Secondary: 68W40.
Key words and phrases. Computational modeling, impedance, structured tree, hemodynamics, pulmonary, respiration.

predictive ability of models that previously assumed static distal hemodynamic behavior.

1.1. **Boundary conditions.** A variety of static boundary conditions have been used to model distal vascular beds, including constant pressure [17], resistance [12], lumped parameter models [5, 6, 33] and geometry-based impedance [4, 15, 23, 25]. While trivial to implement, constant pressure representations are a poor choice in compliant walled models with pulsatile flow for all but a few circumstances where the pressure is steady. The specification of measured pressure or flow waveforms at both inlet and outlet vessels may be problematic if the vessel compliance is not known. Resistance boundary conditions provide an alternative in the form of a constant relationship between pressure and flow. As with pressure, this relationship is not always realistic, including in regions where retrograde flow is present that would lead to negative pressure. While including a region of interest in the model will provide wave propagation properties, without the use of an impedance boundary condition this will only extend to the large vessels included in the region of interest. A resistance boundary condition is unable to include the effects of damping, phase lag and wave propagation that occur in the compliant vessels present in the downstream network [2, 36]. These resistance limitations can be overcome by using an impedance boundary condition. Lumped parameter impedance models have typically been derived from electrical analog circuits comprised of resistors, capacitors and/or inductors fit to experimental data to represent a vascular network [10, 6]. In the absence of data at the outlets, or in predictive models where the modeled region of interest impacts flow distribution, it is difficult to determine reasonable lumped parameters for each outlet. This lumped parameter limitation is addressed by using geometry-based methods to calculate the impedance of a representative vascular geometry (i.e., fractal-like model) using Womersley's method [2, 28, 35]. Such geometries can be directly measured or based on a derived structured tree representing a vascular region [15, 25]. Previous work tailored geometry based impedance boundary conditions to specific vascular regions at specific physiologic states, such as the pulmonary vasculature at inspiration and expiration [4, 23], or viscera, peripheral, and pulmonary vascular beds at rest and exercise [12, 25, 13]. Although impedance boundary conditions may be tuned to accurately represent the pulsatile relationship between pressure and flow over a cardiac cycle, these outlet boundary conditions are static in that they do not change over time to reflect physiologic changes outside of the cardiac cycle.

The representation of dynamic physiology has been presented previously by Marsden et al [13, 12] and Kim et al [11]. In investigations of the effects of respiration on TCPC (total cavo-pulmonary connection) subjects, Marsden, et al [13, 12] incorporated the effects of respiration into the inlet flow. TCPC patients lack a functioning right-heart causing pulmonary flow to be dependent on the venous return and the respiratory and peripheral pumps [14, 29]. Modifying the inlet flow waveform is an effective method for representing the effects of respiration in the compromised Fontan circulation; however, it does not consider the cause, i.e., impedance changes due to arteriole constriction in the lung. In cases where measured flow is used as the inlet boundary condition, the effects of downstream influences, such as impedance changes, cannot be distinguished from driving forces. Therefore, care must be taken when prescribing boundary conditions to ensure that their selection does not unnecessarily influence computational results; particularly when modifications (i.e., treatment planning scenarios) made in one location may influence hemodynamics

in another location. Kim et al [11] incorporates a dynamic boundary condition in a model of the coronary arteries. The inlet boundary condition was specified as a contraction (i.e., pressure increase) in the cardiac tissue to pump blood. This contraction was coupled with the outlet boundary condition of the coronary arteries. This coronary pressure provided feedback to the downstream vascular bed, altering the vascular impedance in the coronary artery beds based on location and cardiac output. This model effectively describes a dynamic boundary condition of the coronary arteries, but does not consider dynamics that are not coupled to the cardiac cycle or inlet boundary condition.

1.2. **Respiration as a feedback mechanism.** In this work, respiration is considered as an example of distal dynamics that is not coupled to the cardiac cycle. While the pulmonary system is not specifically performing a regulatory function with respiration, the arterioles in the pulmonary system are subject to systematic fluctuations in alveolar/arteriolar pressure that result in the modulation of arteriole diameter and pulmonary vascular impedance. The effects of respiration on pulmonary pressure, flow and impedance have been studied for both the healthy [3, 20, 34] and the compromised cardio-pulmonary systems [18, 21]. For the healthy lung, Burton and Patel [3] conducted animal studies for both positive pressure ventilation (PPV) and negative pressure ventilation (NPV) in which they concluded that pulmonary impedance is a variable throughout the respiratory cycle for both ventilation methods. In normal circulation, this change in impedance does not impact the cardiac output due to the ability of the healthy heart to increase driving pressure as required to overcome any increase in impedance. In a compromised cardiopulmonary system, the fluctuations in pulmonary impedance may have a critical effect on both pulmonary pressure and flow, because without a healthy right ventricle to drive against the increased impedance, flow through the pulmonary arteries may diminish, halt or reverse. Therefore, the effects of respiration are critical to the computational analyses of compromised cardio-pulmonary systems and must be considered when using these analyses to assess treatment options.

Models of the pulmonary physiology have been used to investigate pulmonary stenosis and the potential surgical outcomes to resolve the stenosis [23], as well as possible repair options associated with congenital heart defects, such as a Fontan procedure, known as TCPC [6, 12, 17, 22]. However, the majority of pulmonary models have ignored the effects of respiration when incorporating the downstream network. Marsden, et al [12] found that including the effects of respiration produced results that led to a different optimal surgical solution when considering the Fontan circulation.

The objective of this work was to extend the work of Kim et al [11], Marsden et al [13, 12] and Clipp and Steele [4] to develop a time-varying outlet boundary condition for computational analyses that can be used to represent the effects of physiologic regulation or feedback. The pulmonary vasculature was used as the test case for implementation of the dynamic boundary condition.

2. Methods.

2.1. **Experimental data analysis.** In previous work, pulmonary pressure and flow data were collected over multiple cardiac cycles to capture the hemodynamics associated with respiration during PPV in open-chested lambs. The details of the experimental data collection can be found in Clipp and Steele [4]. Pressure and flow

data extracted at maximal inspiration and maximal expiration (Figure 1) were used to compare the effects of respiration. The blood pressure was filtered with a low-pass Butterworth filter with a cutoff frequency of 20 Hz to remove noise. As seen in a representative data set in Figure 1a, blood flow is largely insensitive to respiration, with only a slight change in cardiac cycle length (0.48 and 0.465 seconds for the expired and inspired states, respectively) and no significant change in mean flow or waveform shape. In Figure 1b, respiration is shown to have an impact on mean blood pressure with a 21.5% increase from expiration (15.01 mmHg) to inspiration (18.24 mmHg).

A numerical study to investigate the effects of respiration was performed by the authors [4] using pseudo-dynamic outlet boundary conditions to quantify the relationship between pulmonary geometry, impedance and respiration. In the previous study, several fractal-like geometries were created to represent smaller vessels as they branched from the main pulmonary arteries. The impedance calculated for each of these small artery structures was used as the outlet boundary condition for the large vessel model. Experimental data of pressure and flow in the main pulmonary artery demonstrated that while the periodic flow delivered by the healthy right ventricle was relatively insensitive to respiration, pressure increased with PPV induced inspiration. This data was used to optimize geometric parameters of the fractal-like trees in the exhaled state and then to determine the geometric changes in the resistance vessels ($r \leq 250\mu m$) required to produce the pressure changes observed in the inhaled state. While the previous work quantified the geometric transition required to modulate impedance as observed during respiration, it did not attempt to dynamically model changes associated with respiration as presented by Marsden, et al [13, 12].

Pulmonary impedance was computed using the experimental data for each respiratory state and the resulting modulus and phase are compared in Figures 1c and 1d. Upon examination, it was found that the most significant difference between the two spectra is the zero-frequency modulus (or resistance) component. At maximal expiration and inspiration, the resistance is 609 and 775.5 dynes s cm^{-5} respectively, which corresponds to a 21.5% increase. This is the same increase seen with the mean pressure and suggests that the pressure gain is due to the gain in pulmonary vascular impedance. The higher frequency phase components show larger fluctuations, which may be attributable to the differences seen in the pressure waveforms between expiration and inspiration. From approximately 0.3 to 0.4 seconds the maximal inspiration waveform shows larger fluctuations than the maximal expiration waveform. These differences may be due to noise in the system model and geometry simplification (i.e., loss of reflection points); however, it should be noted that this may also be due to physiologic changes that occur as part of the respiratory process.

2.2. **Time-varying boundary condition.** The total resistance of a vascular network can be predicted from the relationship between the pressure gradient and flow, where the pressure gradient is required to drive the flow through the vascular network. The resistance of a tube can be directly computed and is inversely proportional to vessel diameter [1]. Therefore, if vessel diameter changes with time, so will its resistance. In the case of respiration, arteriole and alveoli dimensions fluctuate as air distends the alveoli. When alveoli are distended during inspiration, vascular resistance increases as shown by the increase in pressure required to drive the same flow through the pulmonary beds.

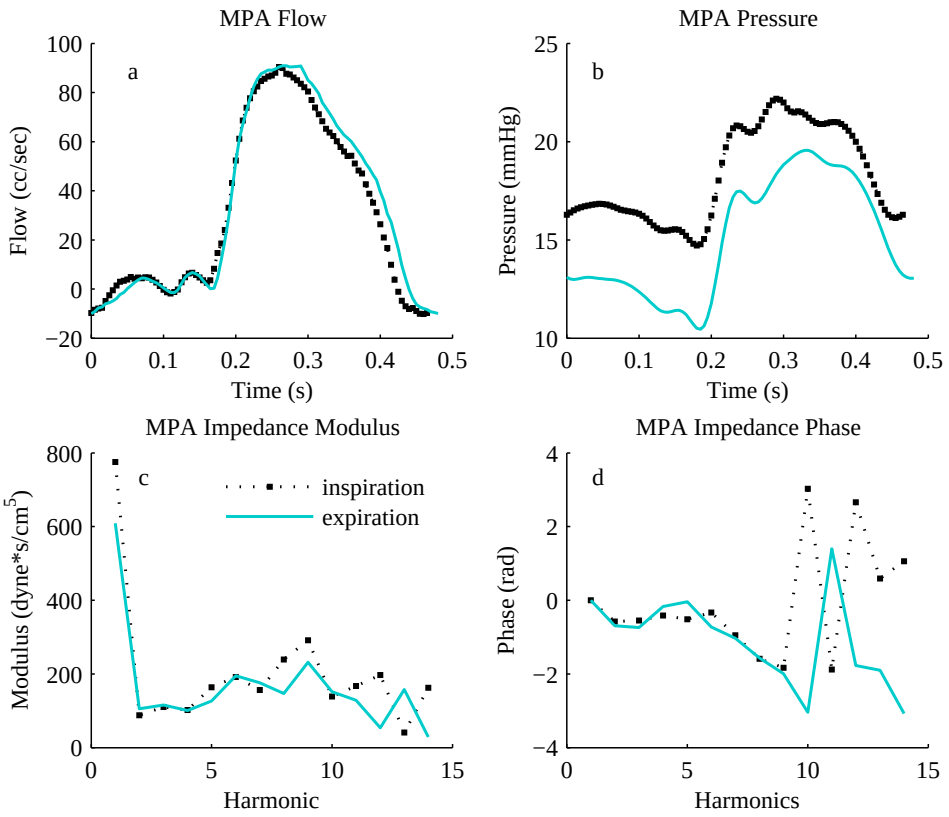

FIGURE 1. Experimental lamb data comparison between maximal expiration and maximal inspiration. The blood flow, blood pressure and impedance modulus and phase for one cardiac cycle are shown for both the maximal expiration and maximal inspiration case in the main pulmonary artery (MPA).

Because the primary difference between the impedance spectra was found in the resistance component, the dynamic boundary condition was focused on the variation of the resistance parameter. The hybrid (TVR-Z) boundary condition is a combination of the time-varying resistance (TVR) and a static impedance (Z) spectrum. Impedance is the pulsatile analog to resistance and incorporates the phase lag and damping observed in compliant networks. The impedance was determined from structured geometric representations of networks of small arteries and capillaries as described in Olufsen et al [16, 15] and Steele, et al [25]. The parameters for the structured-tree geometry were optimized specifically for the pulmonary vasculature in Clipp and Steele [4]. The resistance, or zero-frequency component of impedance, was specified using a linear, time-varying equation to increment the resistance based on an initial and final resistance (R_i, R_f) over a desired number of time steps n,

$$R_k = R_{k-1} + \frac{1}{n}\left(R_f - R_i\right) \tag{1}$$

where R_k is the resistance at the current time step and R_{k-1} is the resistance at the previous time step.

2.3. **Application.**

2.3.1. *Fluids solver.* The TVR-Z boundary condition was implemented in a previously described one-dimensional (1D) finite-element fluids solver [8, 25, 24, 32, 26]. The 1D solver assumes incompressible, Newtonian, axially dominated flow with a parabolic flow profile. Based on the assumptions, appropriate derivations for the conservation of mass (2) and the conservation of momentum (3) equations were found. A third constitutive equation (4) is required to solve for the three unknowns: pressure, flow and area. The ability to model linear and non-linear viscoelastic vessel walls was recently implemented in the current 1D solver [26]. While it is suspect that the pulmonary vessels would exhibit viscoelastic behavior, there is currently not enough data to properly parameterize such models. Therefore, a linear elastic constitutive model was used with the Young's modulus E and wall thickness h specified to be constant.

$$\frac{\partial a}{\partial t} + \frac{\partial q}{\partial z} = 0 \tag{2}$$

$$\frac{\partial q}{\partial t} + \frac{\partial}{\partial x}\left((1+\delta)\frac{q^3}{A}\right) + \frac{a}{\rho}\frac{\partial p}{\partial z} = \xi\frac{q}{a} + \nu\frac{\partial^2 q}{\partial z^2} \tag{3}$$

$$a\left(p(z,t),z\right) = \frac{a_0}{(1-\frac{r_0(z)}{Eh}p(z,t))^2} \tag{4}$$

The above equation variables are defined as: a (cm^2) cross-sectional area, q (cm^3 s^{-1}) volumetric flow rate, p (dynes cm^{-2}) pressure, z (cm) axial location along a vessel and t (s) time. a_0 is the unstressed area and r_0 the unstressed radius of the vessel with respect to the axial location. The parameters δ (dimensionless), and ξ (cm^2) are defined for a profile function, and $\nu = \mu/\rho$ (cm^2/sec) denotes the kinematic viscosity. In this study, a parabolic velocity profile was assumed, such that $\delta = 1/3$ and $\xi = -1.167$. A detailed derivation of this model is described in earlier works [8, 9, 15, 32]. The unstressed radius was estimated to be 86% of the diastolic radius. The Eh term was specified to be 30% of the approximate systemic wall properties, or $Eh = 184$ (mmHg cm) as described in [4]. The fluid properties were defined as density $\rho = 1.05$ (grams cm^{-3}) and kinematic viscosity $\nu = 4.67 \times 10^{-2}$ (cm^2 s^{-1}). Table 1 lists the values for the variables associated with the above equations.

TABLE 1. Equation Constants. The constants used in the appropriately derived equations representing the conservation of mass and momentum and the constitutive equation. Constants noted n.d. are non-dimensional.

Constant	Value	Units
r_o	$0.86 * r$	cm
$E * h$	184	mmHg cm
δ	1/3	n.d.
ξ	-1.167	cm^2
ρ	1.05	g cm^{-3}
ν	4.67×10^{-2}	cm^2 s^{-1}

The outlet impedance boundary condition was obtained by solving the linearized version of the Navier-Stokes equations for a fractal-like structured tree representing a vascular bed distal to the model boundary [25, 16, 15]. This approach was first described by Womersley [36] and Taylor [28]. The impedance, Z, is computed in the frequency domain as a relationship between pressure and flow such that

$$P(z,\omega) = Z(Z,\omega)Q(z,\omega) <==> Q(z,\omega) = P(z,\omega)Y(z,\omega)$$
$$\text{where } Y(z,\omega) = 1/Z(z,\omega).$$

P and Q represent pressure and flow in the frequency domain and Y the admittance. Impedance is a complex array, where the zero frequency term ($\omega = 0$) is the resistance. For the dynamic TVR-Z model, this zero frequency term was updated using the resistance term defined in equation 1. This relationship was used to compute a flow, $\hat{q}$, for a pressure, p, and admittance, y, in the time domain using a convolution

$$\hat{q}(z,t) = \frac{1}{T}\int_{-T/2}^{T/2} y(z,t-\tau)p(z,\tau)d\tau \tag{5}$$

at each model outlet ($z = L$) where T is the period of the cardiac cycle. The flow was evaluated for discrete time points using the number of time steps in a cardiac cycle, N, using the form

$$\hat{q}(n) = \sum_{j=0}^{N-1} y(j)p(n-j). \tag{6}$$

The finite element solution was found by creating a matrix representation, M, of the model using equations 2-3, multiplying the matrix by an array of trial solutions, W, and iterating over trial solutions for each time step until the residual, $\mathcal{R}$, was minimized

$$M \times W = \mathcal{R}. \tag{7}$$

The i^{th}elements in M corresponding to the outlets were therefore found such that

$$\mathcal{R}_{q_i} = q_i^t - \hat{q}_i(p_i^t) = 0, \tag{8}$$

where q_i^t and p_i^t represent the trial solution of the i^{th} element representing the boundary and $\hat{q}_i$ represents the boundary condition flow. For a comprehensive derivation of the finite element solver see [32, 26].

2.3.2. *Pulmonary model.* The pulmonary geometry (Figure 2) from the authors' previous work [4] was analyzed using the pulsatile flow waveforms (unpublished experimental flow), and the dynamic boundary condition for an entire respiratory cycle. The respiratory cycle involves a transition from expiration to inspiration and then a return to the expiratory phase. Although a periodic waveform could have been used, the flow for an entire respiratory cycle was specified at the inlet to include the slight change in period during inspiration. The first cardiac cycle was repeated six times to allow the solver to sufficiently settle before respiration was initialized. A total of 16 cardiac cycles were evaluated with only the cycles after initialization shown. The geometry-based impedance spectra were known from the structured-trees determined in the authors' previous work [4]. The impedance spectra were found using an optimization algorithm to determine the structured-tree parameters at each outlet for both expiration and inspiration, providing the zero-frequency or resistance values. The resistances at expiration and inspiration were defined as R_i and R_f, respectively. The change from expiration to inspiration occurs between $t = 0.92s$ and $t = 1.22s$ in the experimental data set, while the

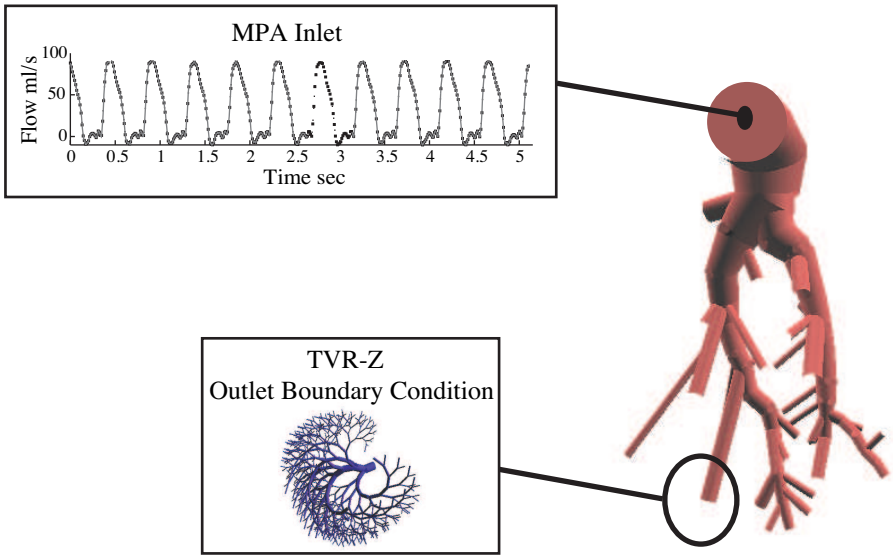

FIGURE 2. Large Vessel Geometry of Computational Models. The pulmonary model consisted of a large-vessel geometry, an inlet boundary condition representing the flow from an entire respiration cycle (over 10 cardiac cycles) and the outlet boundary conditions. The outlet boundary condition was a structured-tree impedance boundary condition with parameters optimized for the pulmonary vasculature with a time-varying resistance component.

return to expiration from inspiration occurs between $t = 1.8s$ and $t = 2.12s$. The pulmonary model was analyzed with a static boundary condition, as well as with dynamic step and linear transitions to investigate the changes in pressure due to varying blood flow, as well as to varying resistance. The step transition provided a demonstration of the ability of the dynamic boundary condition to react quickly, while the linear transition provided a dynamic response on the time scale of the experimental data. A complete respiration cycle was analyzed, beginning with expiration, transitioning to inspiration and then returning to expiration. Table 2 lists the change in resistance for both transitions and the time at which the transition was initialized and completed for one outlet example. The analyses were completed using 200 time steps per cardiac cycle (for a period of 0.48 s) on a 2.4 GHz Intel Core 2 Duo MacBook.

TABLE 2. The transition from expiration to inspiration was completed by scaling the resistance of each outlet. An example of the initialization and completion transition times and the change in resistance for one branch are shown for both the linear and the step transitions.

	Expiration to Inspiration			Inspiration to Expiration		
Transition Type	ΔR	t_i	t_f	ΔR	t_i	t_f
Linear	3911	0.92	1.22	-3127	1.8	2.21
Step	3911	0.92	0.925	-3127	1.8	1.805

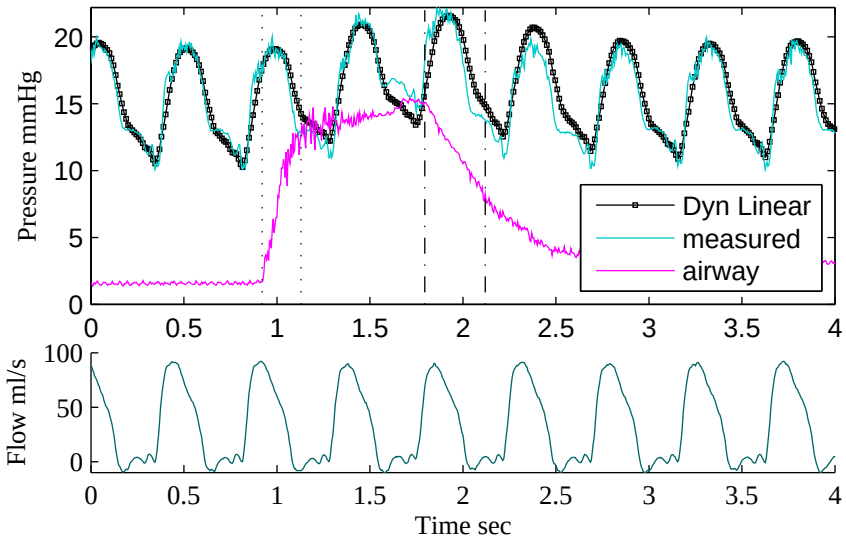

FIGURE 3. Pulmonary Model Results.The predicted linear dynamic and measured main pulmonary artery (MPA) flow and pressure are shown. The respiration curve is also shown, highlighting the increase in blood pressure for both the predicted dynamic and measured data. The dynamic boundary condition is able to represent the changes in vascular impedance caused by respiration.

3. **Results.** The dynamic boundary condition was successfully implemented for the pulmonary model and the inlet pressure was accurately predicted for an entire respiratory cycle. A comparison of the measured and predicted values for blood pressure and blood flow in the main pulmonary artery, as well as the respiratory cycle are shown in Figure 3. The dynamic boundary condition is able to accurately reflect the impedance calculated by the structured-tree and the increased vascular impedance caused by compression of the arterioles by the air-filled alveoli. The dynamic boundary condition is able to react quickly with little delay apparent in the resulting pressure calculation. The return to an expiration state is also completed quickly with little delay in the pressure calculation.

The static boundary condition (parameters optimized to the expiratory phase) was compared to both the step and linear transition dynamic boundary condition, as shown in Figure 4. The results for the static boundary condition analysis demonstrate that the changes in flow that occur between cardiac cycles have an important effect on the pressure and area, despite the relatively minor differences (less than 5%) in cardiac cycle length. This serves to emphasize the importance of including the dynamic changes present due to the cardiac output, as well as distal network regulation.

The step transition dynamic boundary condition analysis demonstrates the slight response time limitation of the numerical solution. The ability of the solver to incorporate a dynamic transition is limited by its ability to reach a stable solution. The initial solution (before transition) required the completion of multiple cardiac cycles to reach a stable solution. After the onset of transition the numerical solution

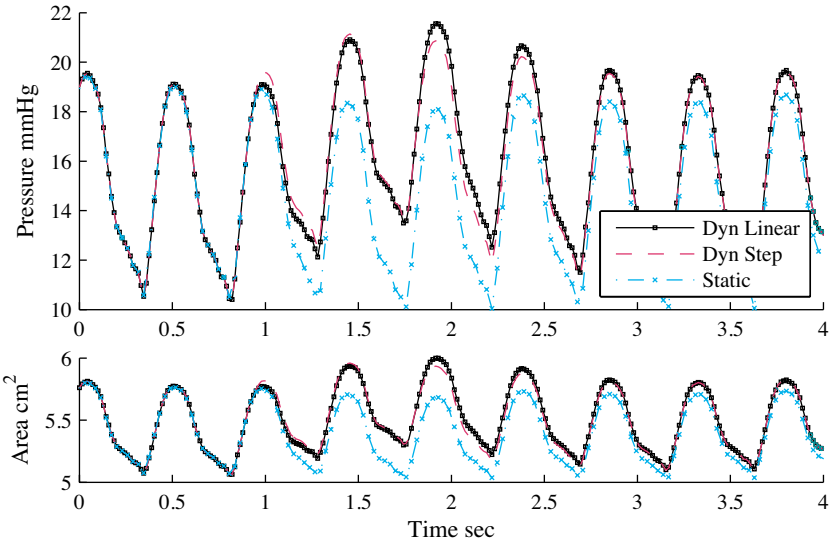

FIGURE 4. Predicted Pulmonary Model Results. A comparison of the linear and step change dynamics and the static model is shown. The predicted static data demonstrates the variation in pressure simply as a result of varying blood flow, but notes the need for varying outlet boundary conditions. The step change shows that a faster response is possible, and that future work must determine the proper dynamic waveform required to model respiration.

begins to acquire instability that manifests as a delay in response time for the resulting pressure and area calculation. As evident by the results of the linear transition dynamic boundary condition analysis, this slight instability does not limit the ability of the numerical solution to react physiologically.

To provide a closer view, the predicted maximal expiration pressure waveforms (the seventh full cardiac cycle) and the predicted maximal inspiration pressure waveform (the fourth full cardiac cycle) are shown with the measured data in Figure 5. The root mean square error was calculated for each state, resulting in an RMS error of $RMS = 0.61$ mmHg and $RMS = 0.59$ mmHg, for expiration and inspiration, respectively. The maximum error for the entire respiratory cycle is located at approximately 1.65 seconds. This error was 1.6 mmHg, which is less than a 10% error. This error is larger than the error found in the remainder of the computational analysis due to the lack of change in the compliance of the large vessels from expiration to inspiration in the computation. This is discussed in more detail in the Limitations and Future Work section of the Discussion.

4. **Discussion.**

4.0.3. *Conclusion and significance.* The dynamic boundary condition was successfully implemented in a model of the pulmonary vasculature. The results of this work demonstrate that a time-varying boundary condition may be used to model pressure changes due to a distal mechanism. The dynamic boundary condition was

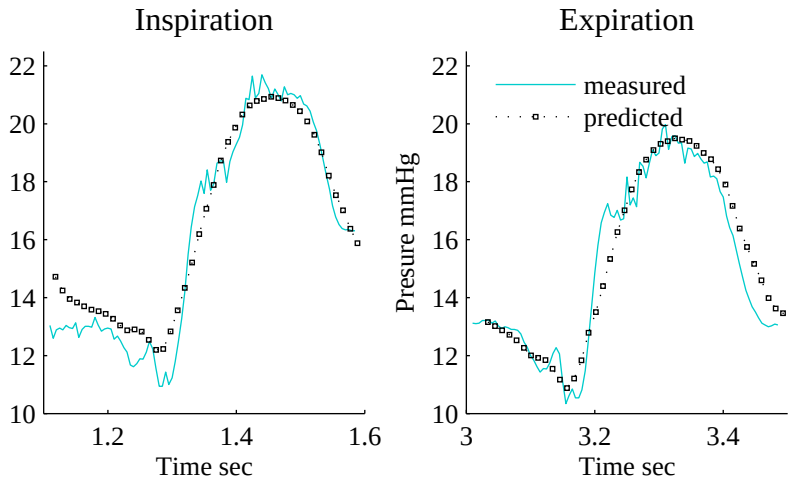

FIGURE 5. Maximal Expiration and Inspiration Pressure Waveforms. Waveforms isolated from the measured and predicted (linear dynamic) data to demonstrate the ability of the boundary conditions to represent the downstream network of vessels during both states of respiration.

able to react quickly to the changes in resistance applied to the model and the predicted pressure waveforms have a minimal error when compared to the measured pressure at each cardiac cycle throughout the respiratory cycle.

This work is significant in that it examines a dynamic boundary condition capable of incorporating organ specific features and demonstrates the importance of including both these dynamic distal effects and those dynamic effects present in the cardiac output. While this model can be extended to describe any organ, the pulmonary system was selected for the initial studies due to the regular, dynamic effects of respiration. This work demonstrates that it is possible to dynamically change the outlet boundary conditions to simulate distal changes in the vascular network and to accurately predict pressure and flow in a region of interest while considering regulatory or feedback mechanisms. It is important to note that models of the Fontan circulation have been analyzed in previous work, but few have included the effects of respiration, most notably Marsden et al [12], which has been discussed previously. Both Marsden et al [12] and the authors believe that a more accurate model of the Fontan circulation can be achieved with the inclusion of respiratory effects.

Spilker et al [23] analyzes a pulmonary model with a pulmonary arterial stenosis and without to determine whether stenosis removal would present a favorable outcome for the patient. The study suggests that the decrease in pressure/increase in flow that would result from the procedure would not warrant the surgical risk. However, Spilker et al [23] does not consider the effects of respiration when considering the surgical outcome. As shown in the Experimental Data Analysis section, the pressure in the main pulmonary artery may increase by 20% during inspiration

and these effects should be considered when evaluating surgical outcomes. This increase in pressure coupled with the stenosis, which would further increase pressure, may result in a different treatment recommendation.

While this study used dynamic outlet boundary conditions to analyze the pulmonary physiology, this method can be applied to all organ systems. Throughout the body, organ systems use feedback mechanisms to regulate blood flow through vessel constriction and/or dilation. The current dynamic boundary condition assumes a time-varying response, however the dynamic change could be modified to utilize a pressure- or flow-varying response. As the pressure in the organ increases or decreases, the resistance could be scaled to reflect a response in the resistance vessels, modulating the pressure as naturally occurs in the organ system.

4.0.4. *Limitations and future work.* One of the limitations of this work was the lack of consideration for any changes in the compliance of large vessels during the respiratory cycle. The large vessels maintained the same pulmonary compliance determined in previous work [4] throughout the entire respiratory cycle. It is clear that a change in compliance for the large vessels is present by the change in pressure gradient between maximal expiration and maximal inspiration, approximately a 1.5 mmHg decrease or a 16% change. Altering the properties of the structured-tree does not provide a substantial change in the pressure gradient nor does changing the resistance of the downstream network. To incorporate this change would require a change in the large vessel properties based on the state of respiration. In the future, when tailoring a dynamic boundary condition to the pulmonary system and the respiratory cycle it will be important to consider the compliance changes in both large vessels described by the constitutive model and the small vessels described by the boundary condition.

A second limitation of this work was found in the experimental data used to develop the pulmonary model. The data was collected from lambs (to represent the pediatric model) intubated and on a ventilator during an open-chest procedure. The differences between positive-pressure ventilation (PPV) and negative-pressure ventilation (NPV) have been considered [3, 20] and it is known that the effects on the hemodynamics of the pulmonary vasculature differ between the two ventilation mechanisms. In the future, NPV data should be assessed to determine normal, free-breathing changes in pulmonary vascular impedance due to respiration. With the addition of NPV hemodynamic and air pressure data, it will be possible to correlate the change in resistance and the change in pulmonary air pressure.

Future work will also use the dynamic boundary condition to assess the implications of surgical intervention to remove a stenosis. This will be compared to Spilker et al [23] to determine whether including respiration in the analysis of options would have impacted the surgical recommendation. In addition to pulmonary stenosis, the dynamic boundary condition will also be used to evaluate the Fontan circulation. This will require a more complex feedback loop that must include changes in passive flow entering the pulmonary circuit, as well as the dynamic changes to impedance caused by respiration.

Acknowledgments. We would like to thank the referees very much for their valuable comments and suggestions.

REFERENCES

[1] A. P. Avolio, *Multi-branched model of the human arterial system*, Medical and Biological Engineering and Computing, **18** (1980), 709–718.

[2] D. J. Brown, *Input impedance and reflection coefficient in fractal-like models of asymmetrically branching compliant tubes*, IEEE Transactions on Biomedical Engineering, **43** (1996), 715–722.

[3] A. C. Burton and D. J. Patel, *Effect on pulmonary vascular resistance of inflation of the rabbit lungs*, Journal of Applied Physiology, **12** (1958), 239–246.

[4] R. B. Clipp and B. N. Steele, *Impedance boundary conditions for the pulmonary vasculature including the effects of geometry, compliance, and respiration*, IEEE Transactions on Bio-Medical Engineering, **56** (2009), 862–870.

[5] M. R. de Leval, G. Dubini, F. Migliavacca, H. Jalali, G. Camporini, A. Redington and R. Pietrabissa, *Use of computational fluid dynamics in the design of surgical procedures: Application to the study of competitive flows in cavo-pulmonary connections*, Journal of Thoracic and Cardiovascular Surgery, **111** (1996), 502–513

[6] D. A. de Zèlicourt, K. Pekkan, J. Parks, K. Kanter, M. A. Fogel and A. P. Yoganathan, *Flow study of an extracardiac connection with persistent left superior vena cava*, The Journal of Thoracic and Cardiovascular Surgery, **131** (2006), 785–791.

[7] B. Flemming, E. Seeliger, T. Wronski, K. Steer, N. Arenz and P. B. Persson, *Oxygen and renal hemodynamics in the conscious rat*, Journal of the American Society of Nephrology, **11** (2000), 18–24.

[8] T. J. R. Hughes and J. Lubliner, *On the one-dimensional theory of blood flow in the larger vessels*, Mathematical Biosciences, **18** (1973), 161–170.

[9] T. J. R. Hughes, "A Study of the One-Dimensional Theory of Arterial Pulse Propagation," Ph.D. Thesis, Report 74–13, Structural Engineering Laboratory, University of California, Berkeley, CA, 1974.

[10] K. Lagana, R. Balossino, F. Migliavacca, G. Pennati, E. L. Bove, M. R. de Leval and G. Dubini, *Multiscale modeling of the cardiovascular system: Application to the study of pulmonary and coronary perfusions in the univentricular circulation*, Journal of Biomechanics, **5** (2005), 1129–1141.

[11] H. J. Kim, I. E. Vignon-Clementel, J. S. Coogan, C. A. Figueroa, K. E. Jansen and C. A. Taylor, *Patient-specific modeling of blood flow and pressure in human coronary arteries*, Annals of Biomedical Engineering, **38** (2010), 3195–3209.

[12] A. L. Marsden, I. E. Vignon-Clementel, F. P. Chan, J. A. Feinstein and C. A. Taylor, *Effects of exercise and respiration on hemodynamic efficiency in CFD simulations of the total cavopulmonary connection*, Annals of Biomedical Engineering, **35** (2007), 250–263.

[13] A. L. Marsden, V. M. Reddy, S. C. Shadden, F. P. Chan, C. A. Taylor and J. A. Feinstein, *A new multiparameter approach to computational simulation for fontan assessment and redesign*, Congenital Heart Disease, **5** (2010), 104–117.

[14] H. Ohuch, Y. Arakaki, Y. Hiraumi, H. Tasato and T. Kamiya, *Cardiorespiratory response during exercise in patients with cyanotic congenital heart disease with and without a fontan operation and in patients with congestive heart failure*, International Journal of Cardiology, **66** (1998), 241–251.

[15] M. S. Olufsen, *A structured tree outflow condition for blood flow in the larger systemic arteries*, The American Journal of Physiology, **276** (1999), H257–H268.

[16] M. S. Olufsen, C. S. Peskin, W. Y. Ki, E. M. Pedersen, A. Nadim and J. Larsen, *Numerical simulation and experimental validation of blood flow in arteries with structured-tree outflow conditions*, Annals of Biomedical Engineering, **28** (2000), 1281–1299.

[17] K. Pekkan, D. A. de Zèlicourt, L. Ge, F. Sotiropoulos, D. Frakes, M. A. Fogel and A. P. Yoganathan, *Physics-driven CFD modeling of complex anatomical cardiovascular flows-a TCPC case study*, Annals of Biomedical Engineering, **33** (2005), 284–300.

[18] D. J. Penny and A. N. Redington, *Doppler echocardiographic evaluation of pulmonary blood flow after the Fontan operation: The role of the lungs*, British Heart Journal, **66** (1991), 372–374.

[19] P. B. Persson, H. Ehmke, H. R. Kirchheim, B. Janssen, J. E. Baumann, A. Just and B. Nafz, *Autoregulation and non-homeostatic behaviour of renal blood flow in conscious dogs*, Journal of Physiology, **462** (1993), 261–273.

[20] F. Petak, G. Albu, E. Lele, Z. Hantos, D. R. Morel, F. Fontao and W. Habre, *Lung mechanical and vascular changes during positive- and negative-pressure lung inflations: Importance of reference pressures in the pulmonary vasculature*, Journal of Applied Physiology, **106** (2009), 935–942.

[21] A. N. Redington, D. Penny and E. A. Shinebourne, *Pulmonary blood flow after total cavopulmonary shunt*, Heart, **65** (1991), 213–217.

[22] D. D. Soerensen, K. Pekkan, D. A. de Zélicourt, S. Sharma, K. Kanter, M. A. Fogel and A. P. Yoganathan, *Introduction of a new optimized total cavopulmonary connection*, The Annals of Thoracic Surgery, **83** (2007), 2182–2190.

[23] R. L. Spilker, J. A. Feinstein, D. W. Parker, V. M. Reddy and C. A. Taylor, *Morphometry-based impedance boundary conditions for patient-specific modeling of blood flow in pulmonary arteries*, Annals of Biomedical Engineering, **35** (2007), 546–559.

[24] B. N. Steele, J. Wan, J. P. Ku, T. J. R. Hughes and C. A. Taylor, *In vivo validation of a one-dimensional finite-element method for predicting blood flow in cardiovascular bypass grafts*, IEEE Transactions on Biomedical Engineering, **50** (2003), 649–656.

[25] B. N. Steele, M. S. Olufsen and C. A. Taylor, *Fractal network model for simulating abdominal and lower extremity blood flow during resting and exercise conditions*, Computer Methods in Biomechanics and Biomedical Engineering, **10** (2007), 39–51.

[26] B. N. Steele, D. Valdez-Jasso, M. Haider and M. S. Olufsen, *Predicting arterial flow and pressure dynamics using a 1D fluid dynamics model with a viscoelastic wall*, SIAM Journal of Applied Mathematics, **71** (2011), 1123–1143.

[27] C. A. Taylor, M. T. Draney, J. P. Ku, D. Parker, B. N. Steele, K. Wang and C. K. Zarins, *Predictive medicine: Computational techniques in therapeutic decision-making*, Computer Aided Surgery, **4** (1999), 231–247.

[28] M. G. Taylor, *The input impedance of an assembly of randomly branching elastic tubes*, Biophysics Journal, **6** (1966), 29–51.

[29] W. B. Troutman, T. J. Barstow, A. J. Galindo and D. M. Cooper, *Abnormal dynamic cardiorespiratory responses to exercise in pediatric patients after fontan procedure*, Journal of the American College of Cardiology, **31** (1998), 668–673.

[30] I. E. Vignon-Clementel, C. A. Figueroa, K. E. Jansen and C. A. Taylor, *Outflow boundary conditions for three-dimensional simulations of non-periodic blood flow and pressure fields in deformable arteries*, Computer Methods in Applied Mechanics and Engineering, **195** (2006), 3776–3796.

[31] I. E. Vignon and C. A. Taylor, *Outflow boundary conditions for one-dimensional finite element modeling of blood flow and pressure waves in arteries. New computational methods for wave propagation*, Wave Motion, **39** (2004), 361–374.

[32] J. Wan, B. N. Steele, S. A. Spicer, S. Strohband, G. R. Feijoo, T. J. R. Hughes and C. A. Taylor, *A one-dimensional finite element method for simulation-based medical planning for cardiovascular disease*, Computer Methods in Biomechanics and Biomedical Engineering, **5** (2002), 195–206.

[33] N. Westerhof, F. Bosman, C. J. De Vries and A. Noordergraaf, *Analog studies of the human systemic arterial tree*, Journal of Biomechanics, **2** (1969), 121–143.

[34] J. L. Whittenberger, M. McGregor, E. Berglund and H. G. Borst, *Influence of state of inflation of the lung on pulmonary vascular resistance*, Journal of Applied Physiology, **15** (1960), 878–882.

[35] J. R. Womersley, *Oscillatory flow in arteries: The constrained elastic tube as a model of arterial flow and pulse transmission*, Physics in Medicine and Biology, **2** (1957), 178–187.

[36] J. R. Womersley, *Oscillatory motion of a viscous liquid in a thin-walled elastic tube. I. The linear approximation for long waves*, The Philosophical Magazine (7), **46** (1955), 199–221.

Received February 2, 2011; Accepted August 24, 2011.

E-mail address: rclipp@gmail.com
E-mail address: bnsteel@ncsu.edu